COMMUNICATION

Crystallization behaviors of Zn_xSb_{100-x} thin films for ultralong data retention phase change memory applications

Yimin Chen,[a] Guoxiang Wang,[a] Xiang Shen,*[a] Tiefeng Xu,*[a] R. P. Wang,[b] Liangcai Wu,[c] Yegang Lu,[a] Junjian Li,[a] Shixun Dai[a] and Qiuhua Nie[a]

Zn_xSb_{100-x} films with low Zn content are crystallized in a single-step process with Sb, while the film (Zn/Sb ratio is about 1:1) exhibits a two-step crystallization process with ZnSb metastable and stable phases. Importantly, ZnSb films have higher crystallization temperature (~257 °C), larger crystalline activation energy (~5.63 eV), better 10 year-data-retention (~201 °C) and lower melting temperature (~500 °C).

Although flash memory has been commercially successful as one of the most popular options for memory applications, it is restricted by its physical limitation beyond the 22 nm technology node.[1] Intensive investigations have been performed to search for new materials to replace flash memory for application in the next-generation nonvolatile Q4 memory. The most promising phase-change material should exhibit reversible crystallization from an amorphous to a crystalline phase and *vice versa*. The changes in optical or electrical properties of phase change materials induced by electrical or laser pulses should be notable enough to meet the requirements for the application in phase change memory (PCM).[2]

So far, Te-based chalcogenide alloys, such as Ge–Te, Sb–Te, Ge–Sb–Te, *etc.*, have been well studied. According to the Ge–Sb–Te ternary alloy phase diagram,[3] the alloys with the composition lying on the GeTe–Sb_2Te_3 pseudo-line, for example, $Ge_2Sb_2Te_5$ (GST), exhibit excellent electrical and structural properties as storage media in PCM. However, there are some critical issues that remain to be solved. During the RESET process from a crystalline to an amorphous state, high melting temperature (~620 °C) and low resistance of the crystalline state could induce a larger RESET current in PCM devices, leading to higher power consumption.[4] In addition, low crystallization temperature (~160 °C) could lead to the instability with a data retention capability of ten years at a maximum temperature of 85–110 °C,[5–7] which cannot meet the requirements of archival life for consumer products and automotive systems (above 120 °C). More importantly, the presence of Te element is toxic and environmentally unacceptable, and high mobility of the Te element could induce the variation in chemical stoichiometry and irreversible segregation.[8]

Recently, tellurium-free phase change alloys, such as Ge–Sb,[9,10] Si–Sb,[11] Ga–Sb,[12–14] Mg–Sb,[15] Sn–Sb,[16] and In–Sb,[17] have been intensively reported. The results revealed that the alloys exhibited fast switching speed due to the growth-dominated crystallization mechanism and possessed suitable phase-change properties for data storage. Nevertheless, there are some drawbacks for these materials. For instance, Ga–Sb films have high melting temperature and small resistance ratio, leading to high power consumption and poor ON/OFF ratio.[18] Mg–Sb films possess relatively low crystallization temperature and are easily phase-separated, resulting in bad thermal stability and short archival life.[15] Previously, we investigated Zn–Sb_2Te ternary alloys, and the results showed that they exhibited larger resistance change, faster crystallization speed, and better thermal stability due to the formation of the amorphous Zn–Sb phase as well as the uniform distribution of Sb_2Te crystalline grains.[19] Thus, it is naturally expected that Zn–Sb bonds could exist in Te-free Zn_xSb_{100-x} films, and the presence of Zn–Sb bonds could enhance thermal stability of phase change materials. To confirm these, we prepared numbers of binary Zn_xSb_{100-x} films with different chemical compositions and investigated their microstructure *via* various diagnostic tools including X-ray diffraction (XRD), X-ray photoelectron spectroscopy (XPS), Raman scattering and transmission electron microscopy (TEM). Furthermore, we evaluated the thermal and electrical properties and examined their correlation with the microstructure of the films.

[a] Laboratory of Infrared Material and Devices, Advanced Technology Research Institute, Ningbo University, Ningbo 315211, China. E-mail: shenxiang@nbu.edu.cn, xutiefeng@nbu.edu.cn; Fax: +86 0574 97600946; Tel: +86 0574 87600947
[b] Laser Physics Centre, Australian National University, ACT, Canberra, 0200, Australia
[c] Shanghai Institute of Micro-system and Information Technology, Chinese Academy of Sciences, Shanghai 200050, China

Table 1 The sputtering parameters and the compositions of Zn_xSb_{100-x} films

Power (W)		Composition	Power (W)		Composition
ZnSb	Sb	(at.%)	ZnSb	Zn	(at.%)
50	30	$Zn_{21.9}Sb_{78.1}$	50	0	$Zn_{49.3}Sb_{50.7}$ (ZnSb)
50	25	$Zn_{24.5}Sb_{75.5}$	50	4	$Zn_{57.7}Sb_{42.3}$
50	15	$Zn_{28.6}Zn_{71.4}$			
50	12	$Zn_{35.2}Sb_{64.8}$			
50	8	$Zn_{40.2}Sb_{59.8}$			
50	5	$Zn_{46.5}Sb_{53.5}$			

We aimed at exploring possible applications of the Zn_xSb_{100-x} film as a PCM device layer.

Zn_xSb_{100-x} films with a thickness of around 120 nm were prepared by magnetron co-sputtering using separated ZnSb and Sb (or Zn) targets on SiO_2/Si (100) and quartz substrates. The chamber was evacuated to 2×10^{-4} Pa, and then Ar gas was introduced to 0.35 Pa for film deposition. A GST film with the same thickness was also prepared for comparison. The film compositions were controlled by adjusting the sputtering power of targets. The concentration of Zn in the as-deposited films was examined using energy dispersive spectroscopy (EDS), and the results were listed in Table 1. The melting temperature of Zn_xSb_{100-x} films was measured using a differential scanning calorimeter (DSC) at a scanning rate of 10 K min^{-1} under the protection of a flowing N_2 atmosphere. Sheet resistance of the films as a function of

temperature (non-isothermal) or time at specific temperatures (isothermal) was *in situ* measured in vacuum at a fixed heating rate of 40 K min^{-1}. The structure of as-deposited and annealed Zn_xSb_{100-x} films was analyzed using XRD, XPS, Raman spectroscopy, and TEM.

Sheet resistance of Zn_xSb_{100-x} and GST films as a function of measurement temperature is shown in Fig. 1(a). Some distinguishable features include: (1) for each film, the sheet resistance gradually decreases with increasing temperature until it reaches an abrupt drop at T_c. The amorphous/crystalline resistance ratio of Zn_xSb_{100-x} films was maintained at around 10^5 during the crystallization process. Compared with GST films, Zn_xSb_{100-x} films have a higher resistance of the crystalline state that increases with increasing Zn concentration. T_c value of Zn_xSb_{100-x} films goes up from ~196 °C to ~270 °C with increasing Zn concentration, all of which are higher than that of GST films (~168 °C). Therefore, Zn_xSb_{100-x} films with a high T_c can be expected to have better thermal stability, which is very important for PCM applications at high temperatures; (2) the change in the sheet resistance across the first crystallization temperature in both Zn_xSb_{100-x} and GST is sharp when the films transform from an amorphous to a crystalline state, indicating that the Zn_xSb_{100-x} films could have a similar faster crystallization speed as the GST film; (3) there is a second resistance drop in ZnSb and $Zn_{57.7}Sb_{42.3}$ films at ~310 °C and ~324 °C, respectively, suggesting a multi-level phase-change process in ZnSb and $Zn_{57.7}Sb_{42.3}$ films.
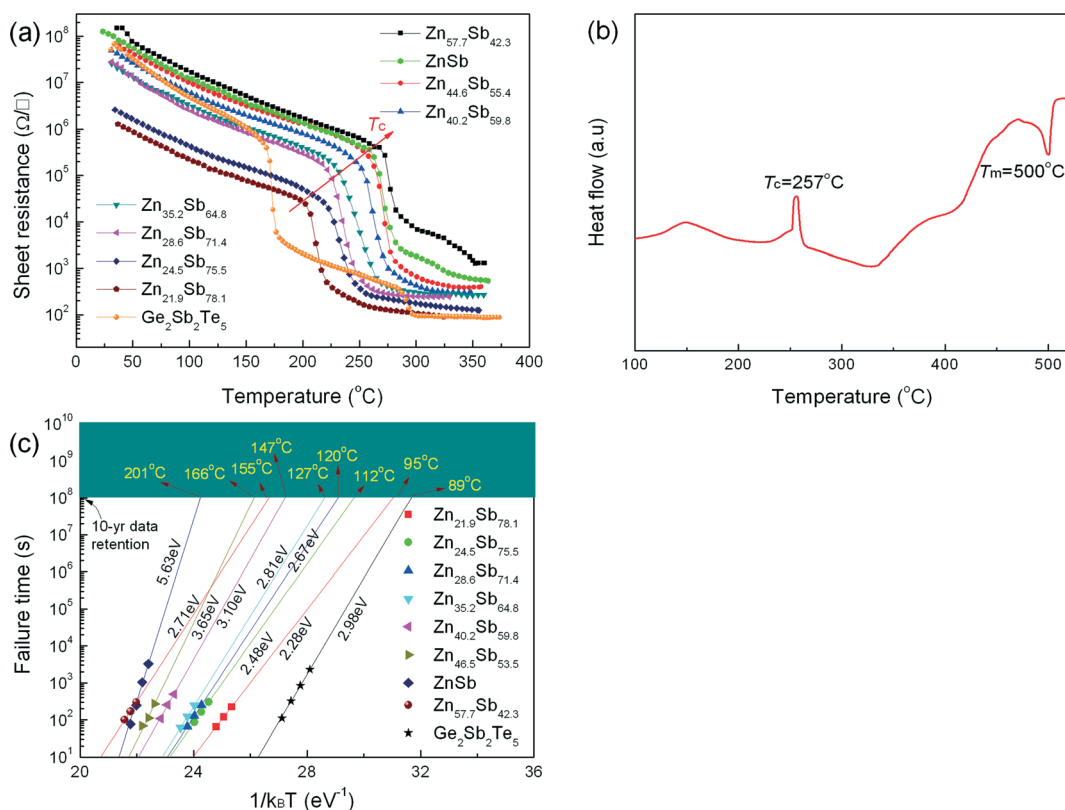
Fig. 1 (a) Sheet resistance of Zn_xSb_{100-x} films as a function of temperature with a heating rate of 40 K min^{-1}; (b) the DSC curve of ZnSb film at a heating rate of 10 K min^{-1}; (c) Arrhenius plots of failure time *vs.* 1/k_BT for GST and Zn_xSb_{100-x} films; 10 year data retention temperatures and E_a can be calculated from the curves.
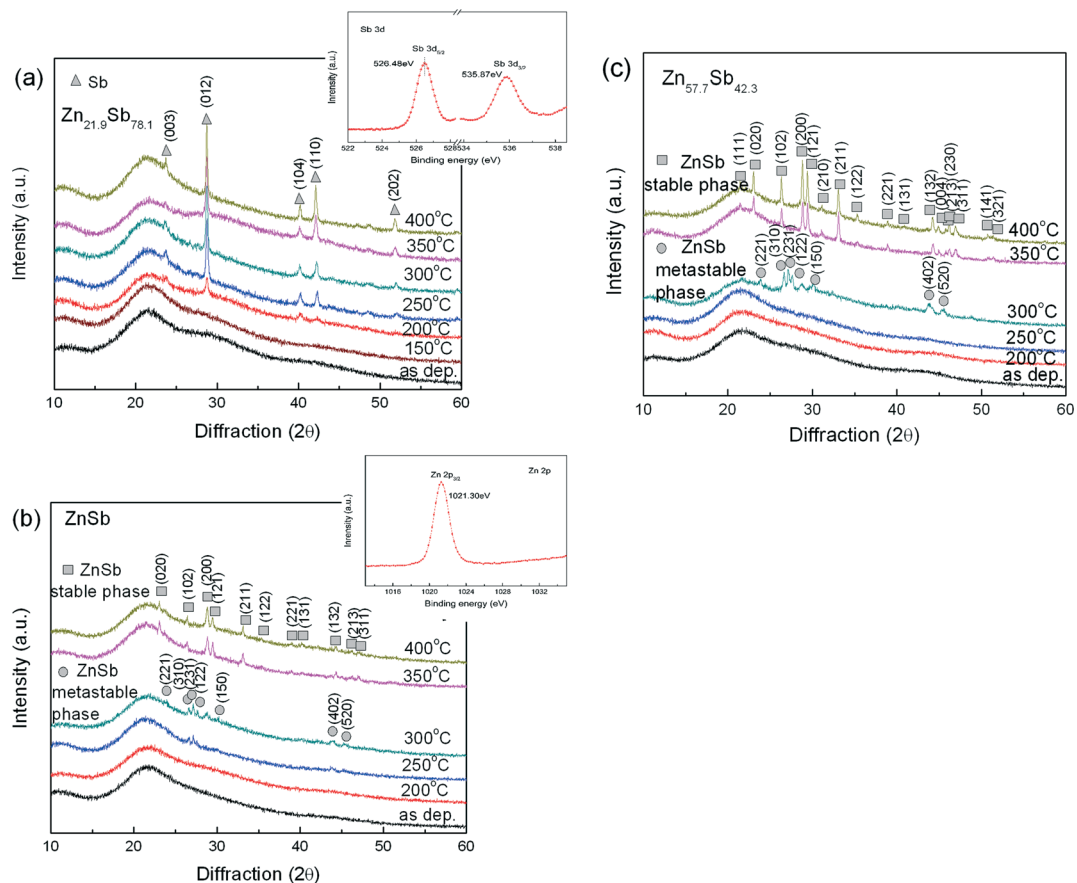
Fig. 2 XRD patterns of Zn_xSb_{100-x} films annealed at different temperatures for 3 min: (a) $Zn_{21.9}Sb_{78.1}$, (b) ZnSb, and (c) $Zn_{57.7}Sb_{42.3}$, respectively; insets are the XPS spectra of $Zn_{21.9}Sb_{78.1}$ and ZnSb films annealed at 300 °C for Sb 3d and Zn 2p, respectively.
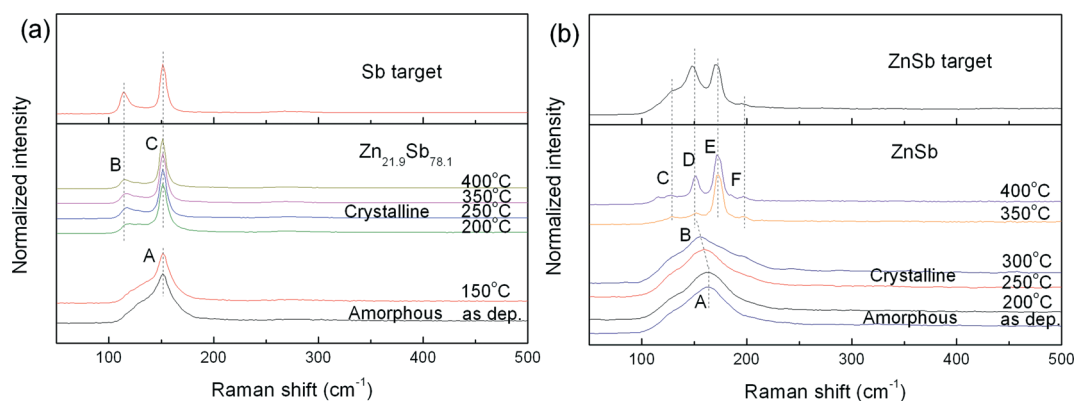
Fig. 3 Raman spectra of (a) $Zn_{21.9}Sb_{78.1}$ and (b) ZnSb films annealed at different temperatures.

Therefore, PCM devices using ZnSb and $Zn_{57.7}Sb_{42.3}$ films could realize three-state storage in one PCM cell employing the resistivity difference among the amorphous, metastable and stable phases in the ZnSb and $Zn_{57.7}Sb_{42.3}$ films. That is to say, three bits data, such as '0', '1', and '2', could be stored in one memory cell in the PCM application.

The melting temperature of Zn_xSb_{100-x} films was measured, and the typical DSC curve for ZnSb is shown in Fig. 1(b). T_c and the melting temperature (T_m) were determined to be ~257 °C and ~500 °C, respectively. T_c value is in

excellent agreement with that from the R-T test, but T_m is relatively lower than that of GST (~620 °C). Higher resistance of the crystalline state and lower melting point are two crucial parameters for reducing RESET current in PCM applications. Therefore, memory devices based on ZnSb films can be expected to have lower power consumption.

Data retention, another important parameter for PCM application, was characterized by extrapolating the isothermal Arrhenius plot of the logarithm of failure time *vs.* the reciprocal of isothermal temperature. Fig. 1(c) is the best fit of failure

vs. reciprocal temperature ($1/k_BT$) using the Arrhenius equation: $t = \tau \exp(E_a/k_BT)$, where t is the time to failure, τ is a proportional time constant, E_a is the crystalline activation energy and k_B is Boltzmann's constant, respectively.[20] As shown in the figure, E_a and 10 year data retention of Zn_xSb_{100-x} films increase obviously with increasing Zn concentration. The 10 year data retention temperatures of all Zn_xSb_{100-x} films are higher than that of GST. Especially, when the ratio of Zn/Sb reaches 1:1, ZnSb film exhibits high E_a (~5.63 eV) and ultralong data retention ability (~201 °C) which are sufficient for the potential applications in automotive electronics (at least 10 years at 120 °C).[21] Nevertheless, when the Zn concentration is more than 50%, it is found that both E_a and 10 year data retention temperature decrease. Therefore, a Zn/Sb ratio of 1:1 can be considered one of the best compositions in a Zn_xSb_{100-x} system.

To investigate the crystallization of the Zn_xSb_{100-x} films, the films were annealed in Ar ambient at different temperatures (in the range of 200 °C to 400 °C) for 3 min and slowly cooled down to room temperature. The structure of the as-deposited and thermal-annealed films was then measured from XRD patterns. It was found that, when Zn concentration is less than 50%, no sharp diffraction peak can be observed in the XRD patterns of the as-deposited Zn_xSb_{100-x} films, and the amorphous phase can be stabilized at an annealing temperature of up to 150 °C for $Zn_{21.9}Sb_{78.1}$ film, 200 °C for $Zn_{24.5}Sb_{75.5}$, $Zn_{28.6}Zn_{71.4}$, and $Zn_{35.2}Sb_{64.8}$ films, and 250 °C for $Zn_{40.2}Sb_{59.8}$ and $Zn_{46.5}Sb_{53.5}$ films. This indicates that the amorphous thermal stability is improved with increasing Zn

concentration. After all the films are crystallized, only peaks corresponding to a single Sb rhombohedral phase can be observed and their intensity gradually decreases with increasing Zn content. A typical XRD pattern for $Zn_{21.9}Sb_{78.1}$ film is shown in Fig. 2(a), and the inset is its XPS Sb 3d spectrum. The binding energies of Sb $3d_{5/2}$ and Sb $3d_{3/2}$ are located at 526.48 eV and 535.87 eV for $Zn_{21.9}Sb_{78.1}$ film, respectively, which are about 2.02 eV and 2.13 eV lower than metal Sb–Sb binding energies.[12] It is well known that the negative shift of the binding energy increases with the decrease of neighboring atom electro-negativity from Sb (2.05) to Zn (1.6).[21] Therefore, the decrease of the binding energy of Sb 3d is due to the fact that parts of the Sb atoms in Sb–Sb bonds are replaced by Zn atoms, forming Zn–Sb bonds. The amorphous Zn–Sb content around crystalline Sb grains serves as centers for suppression of the amorphous-to-rhombohedral phase transition.

Fig. 2(b) and (c) show the XRD patterns for ZnSb and $Zn_{57.7}Sb_{42.3}$ films, and the inset of Fig. 2(b) is a Zn XPS 2p spectrum. ZnSb film was found to maintain an amorphous phase up to 200 °C and then exhibit a two-step crystallization process: amorphous → ZnSb metastable phase at around 250 °C and ZnSb metastable → ZnSb stable phase at around 350 °C. The corresponding phase can be indexed in the XRD database as JCPDS no. 40-809 and JCPDS no. 5-714. Meanwhile, the Zn 2p3/2 peak at 1021.3 eV as shown in the inset of Fig. 2(b) is 0.3 eV higher than metal Zn–Zn binding energies,[22] again confirming that Zn is bonded with Sb. With further increasing Zn content in Fig. 2(c), the diffraction peaks of the crystallized phases in $Zn_{57.7}Sb_{42.3}$ film appear to
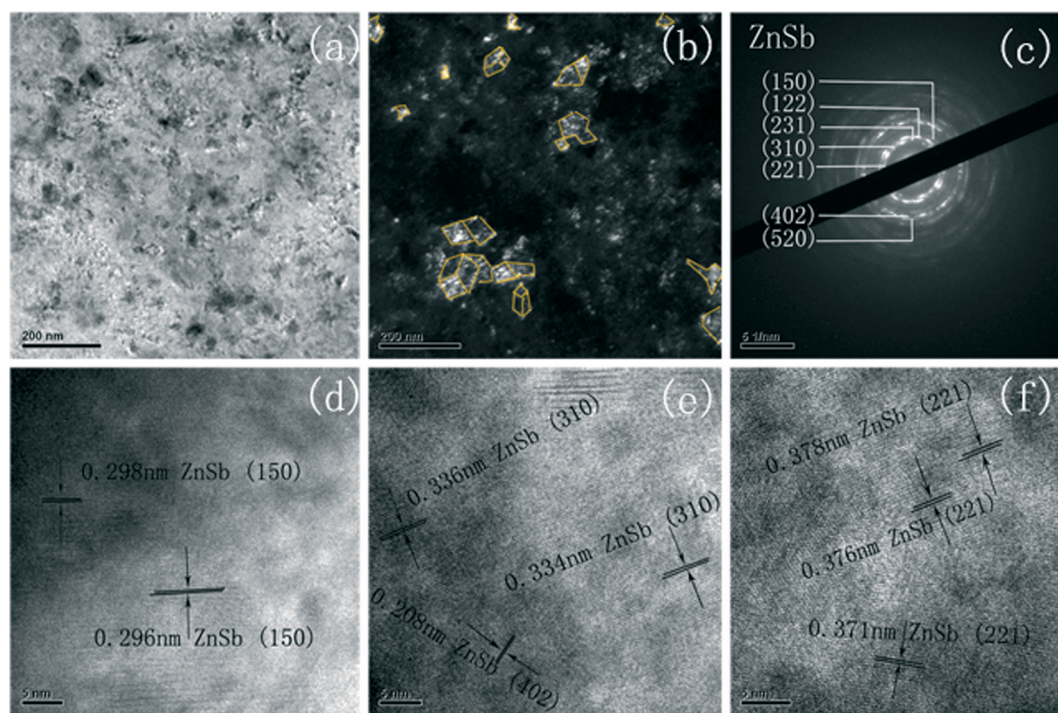
Fig. 4 (a) The TEM BF micrograph, (b) TEM DF micrograph, and (c) SAED pattern of a ZnSb film annealed at 300 °C; (d), (e) and (f) the HRTEM images of the same film.

be sharper in intensity compared with those in Fig. 2(b), implying that the ZnSb crystal grains are becoming larger.

Raman spectra of the as-deposited and annealed $Zn_{21.9}Sb_{78.1}$ and ZnSb films are shown in Fig. 3(a) and (b), respectively. A relatively strong peak at 151 cm^{-1}, which is assigned to the vibration of amorphous Sb–Sb bonds,[23] is overlapping with a broad band in the range from 110 to 180 cm^{-1} (marked as A) in the as-deposited $Zn_{21.9}Sb_{78.1}$ film, and the feature changes into two sharp peaks (ascribed as peaks B and C) when the film is annealed at a temperature from 200 °C to 400 °C. These two sharp peaks have the same positions as those in the Sb target as shown in Fig. 3(a), indicating that the films annealed at high temperatures contain a crystalline Sb phase which is in excellent agreement with the results from XRD measurements. In contrast, ZnSb film exhibits different behaviors. The broad band in the range from 110 to 180 cm^{-1} (marked as A) in the as-deposited film persists well until the film is annealed at a temperature up to 200 °C, and then slightly shifts to a low wavenumber (marked as B in Fig. 3(b)) with increasing annealing temperature from 250 °C to 300 °C. The feature B corresponds to the metastable ZnSb phase although their Raman peaks are not so sharp. This is consistent with the XRD results in Fig. 2(b), where the XRD peaks of the crystallized phases are weak, which might be due to smaller crystalline grains in the film. However, with further increasing annealing temperature, a series of sharp peaks marked as C, D, E and F can be observed and these peaks have the exact same positions as those in the ZnSb target. The two-step crystallization process is in agreement with those found in Fig. 1(a) and 2(b).

Fig. 4(a) and (b) show bright field (BF) and dark field (DF) TEM images for the 300 °C-annealed ZnSb film, respectively. It was found that the film displays many crystalline grains in the BF picture with a size of 20–80 nm, which is in good agreement with that estimated from the line-width of XRD patterns. In the DF picture, the bright regions are assigned to rhombohedral ZnSb crystalline grains as indicated by yellow dotted lines, and sharp polycrystalline rings appear in the SAED pattern of the film as shown in Fig. 4(c). Fig. 4(d)–(f) show high-resolution transmission electron microscopy (HRTEM) images of the same film recorded at different areas. From the interplanar distance, preferred (150), (310), (402) and (221) orientations in the metastable ZnSb phase are evident as marked in Fig. 4(d)–(f). Again, these grain orientations are in excellent agreement with those observed in Fig. 2(b).

Conclusions

In summary, Zn_xSb_{100-x} films with higher T_c, larger E_a, and better data retention ability compared with GST have been confirmed using various diagnostic tools. Especially, when the ratio of Zn/Sb is 1 : 1, ZnSb films have an ultralong 10 year data retention at ~201 °C. Moreover, the higher resistance of its crystalline state and lower melting temperature (~500 °C) could result in a decrease in RESET current and energy consumption of ZnSb-based PCM devices. XRD, XPS, Raman,

and TEM analyses revealed that the ZnSb film undergoes a two-step crystallization process and the precipitate crystal grains are rhombohedral ZnSb. All these excellent properties open up huge potentials of the ZnSb film as one of the best phase-change materials.

Acknowledgements

Notes and references

1   G. J. Meijer, *Science*, 2008, **319**, 1625.
2   M. Wuttig, *Nat. Mater.*, 2005, **4**, 265.
3   M. Wuttig and N. Yamada, *Nat. Mater.*, 2007, **6**, 824.
4   S. W. Ryu, H. K. Lyeo, J. H. Lee, Y. B. Ahn, G. H. Kim and C. H. Kim, *Nanotechnology*, 2011, **22**, 254005.
5   Y. F. Gu, Y. Cheng, S. N. Song, T. Zhng, Z. T. Song, X. Y. Liu, X. F. Du, B. Liu and S. L. Feng, *Scr. Mater.*, 2011, **65**, 622.
6   Y. Sutou, T. Kamada, M. Sumiya, Y. Satio and J. Koike, *Acta Mater.*, 2012, **60**, 872.
7   M. Zhu, L. C. Wu, Z. T. Song, F. Rao, D. L. Cai and C. Peng, *Appl. Phys. Lett.*, 2012, **100**, 122101.
8   L. Krusin-Elbaum, J. C. Cabral, K. N. Chen, M. Copel, D. W. Abraham, K. B. Reuter, S. M. Rossnagel, J. Bruley and V. R. Dline, *Appl. Phys. Lett.*, 2007, **90**, 141902.
9   S. M. Wiggins, J. Solis and C. N. Afonso, *Appl. Phys. Lett.*, 2004, **84**, 4445.
10 S. Raoux, C. Cabral, L. Krusin-Elbaum, J. L. Jordan-Sweet, K. Virwani, M. Hitzbleck, M. Salinga, A. Madan and T. L. Pinto, *J. Appl. Phys.*, 2009, **105**, 064918.
11 T. Zhang, Z. T. Song, F. Wang, B. Liu and S. L. Feng, *Appl. Phys. Lett.*, 2007, **91**, 222102.
12 Y. G. Lu, S. N. Song, Z. T. Song and B. Liu, *J. Appl. Phys.*, 2011, **109**, 064503.
13 P. C. Chang, H. W. Huang, C. C. Chang, S. C. Chang, M. J. Tsai and T. S. Chin, *Thin Solid Films*, 2013, **10**, 1016.
14 C. C. Chang, T. R. Yew and T. S. Chin, *CrystEngComm*, 2011, **13**, 5642.
15 C. C. Chang, C. Y. Hung, K. F. Kao, M. J. Tsai, T. R. Yew and T. S. Chin, *Thin Solid Films*, 2010, **518**, 7403.
16 F. Rao, Z. T. Song, K. Ren, X. L. Li, L. C. Wu, W. Xi and B. Liu, *Appl. Phys. Lett.*, 2009, **95**, 032105.
17 L. van Pieterson, M. van Schijndel, J. Rijpers and M. Kaiser, *Appl. Phys. Lett.*, 2003, **83**, 1373.
18 Y. G. Lu, Z. H. Zhang, S. N. Song, X. Shen, G. X. Wang, L. M. Cheng, S. X. Dai and Z. T. Song, *Appl. Phys. Lett.*, 2013, **102**, 241907.

19 X. Shen, G. X. Wang, R. P. Wang, S. X. Dai, L. C. Wu, Y. M. Chen, T. F. Xu and Q. H. Nie, *Appl. Phys. Lett.*, 2013, **102**, 131902.

20 M. Wuttig and C. Steimer, *Appl. Phys. A: Mater. Sci. Process.*, 2007, **87**, 411.

21 G. X. Wang, Q. H. Nie, X. Shen, R. P. Wang, L. C. Wu, J. Fu, T. F. Xu and S. X. Dai, *Appl. Phys. Lett.*, 2012, **101**, 051906.

22 B. R. Strohmeier and D. M. Hercules, *J. Catal.*, 1984, **86**, 266.

23 E. Cho, S. Yoon, H. R. Yoon and W. Jo, *J. Korean Phys. Soc.*, 2006, **48**, 1616.